Journal of Materials Education Vol. 38 (1-2): 1-14 (2016)

RESEARCH-INFORMED EDUCATION IN MATERIALS SCIENCE AND ENGINEERING: A CASE STUDY

D.J. Browne*, M. Tong, P. Meagher, A.G. Murphy

School of Mechanical and Materials Engineering, University College Dublin,
Belfield, Dublin 4, Ireland.
* *corresponding author: David J. Browne, david.browne@ucd.ie*

ABSTRACT

A course in Metals Processing, delivered to senior engineering students, in which much of the curriculum consists of summaries of selected relevant research projects, is presented. A balanced research team, under the leadership of the course co-ordinator, has designed and delivered an advanced module covering the near net shape processing of metallic alloys. The topics covered include alloy solidification and casting, plasticity and metal forming, and a practical laboratory exercise. Details of the course content, and the research on which much of it is based, are hereby presented, along with commentary on the pedagogic rationale for the approach taken.

Keywords*: teaching and learning; metals processing; alloy solidification; plasticity; microstructural evolution.*

INTRODUCTION

Investment of time in research can yield dividends in the teaching aspects of academic life. This example is in the broad field of Materials Science and Engineering. A research group has designed and delivered a course to final year undergraduate or masters-level engineering students, entitled *Advanced Metals Processing*. In this way a relatively large group of students has the opportunity to learn about selected recent research advances in the area. The team comprises a faculty member who serves as module co-ordinator and is also the research group director, a research fellow, a postdoctoral researcher, and a PhD student. The team thus represents the typical make-up of a small research group. Some of the introductory lecture material is quite standard – of the type found typically in textbooks – but much of the content is gleaned from the results of the research being carried out in the group. In many cases such content is from conference papers which have recently been presented. The research projects have been funded from a variety of sources, including the European Commission, the European Space Agency, and Enterprise Ireland.

In terms of learning outcomes, on successful completion of this subject the student should be able to: 1. link very demanding engineering

service requirements to new high performance materials and processing routes; 2. plan economical process schedules for near-net shape components with minimal environmental impact; 3. design capital equipment for plastic deformation and solidification processing of advanced metallic materials including glasses, composites, smart, and gradient materials; 4. engineer microstructure into materials in order to tailor their physical properties.

This paper presents some research-led course material on metal forming, alloy solidification, and casting processes. The students also complete a laboratory-based exercise, on bulk metallic glasses.

ALLOY SOLIDIFICATION

Essential in metallurgy is that students have a clear understanding of solidification processes, as metallic components – cast metals in particular – derive much of their mechanical strength, as well failure-inducing defects, during the liquid-solid phase transformation. While versions of the casting process can be traced back several thousand years[1] and the understanding that the internal structure and geometry have a major effect on the strength of castings has been known for over 150 years[2], in depth scientific research into the physics of solidification only achieved real focus in the last 60 years[3]. Since that time, huge advances in computational capability, combined with sophisticated experimental techniques, e.g. X-ray diffraction, topography, tomography, and radiography, have led to a significant increase in our understanding of the fundamental physical processes inherent during solidification, and the factors that may be controlled to produce components with superior mechanical properties.

Of all the modern experimental techniques recently developed, *in situ* X-ray radiography has emerged as one of the most important to materials scientists, providing real-time observations of dynamic, and early onset, micro- and macro-scale solidification phenomena in metallic systems[4,5], largely unobtainable through traditional post-mortem metallographic inspection. We have been actively involved in research in this area, and have used our findings in the lectures. Figure 1(a) shows the general principle of the *in situ* X-ray monitoring experimental configuration. The sample material, contained within a specially designed furnace[6], is positioned in the path of an X-ray beam of sufficient energy to provide absorption contrast between high-density and low-density regions within the field-of-view (FOV). The transmitted X-ray beam thereafter projects an image onto a scintillator, converting X-ray photons into visible light photons, which are then recorded by a visible light camera, an example of which, using the Al-Cu system, is shown in Fig. 1(b). Aluminium-rich equiaxed crystals appear brighter in the field-of-view (FOV) as they provide less attenuation of the incident X-ray beam (low-density). Conversely, the copper-rich liquid, owing to the higher density copper, absorbs more of the incident X-ray photons thus producing darker regions in the FOV. Figure 1(c) shows a qualitative 3D reconstruction of the highlighted equiaxed grain in Fig. 1(b), illustrating the variation of solid through the thickness of the sample.

The benefit of *in situ* X-radiography to the materials science classroom is clear. Real-time and direct observations of crystal growth allow students to explicitly observe grain nucleation, grain rotation, solute partitioning, etc., as well as the effects of buoyant grain motion on crystal growth during solidification. For example, while phase diagrams are extremely important in materials science, and provide invaluable information on thermodynamically stable temperature-composition dependent phases, they provide little insight into the kinetics of crystal formation, grain nucleation density, segregation, etc., i.e. dynamic solidification phenomena. Fig. 2 shows an annotated hypoeutectic portion of the Al-Cu phase diagram[7], with a copper concentration of 20wt% highlighted. To date, a significant number of *in situ* X-radiography studies of solidification have been performed using Al-20wt%Cu alloy system[8–10], owing to the high image contrast

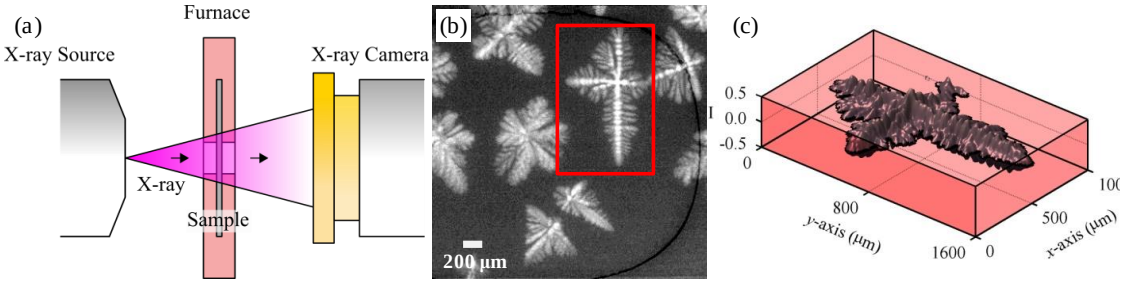

Figure 1. (a) Schematic illustration of *in situ* X-radiography experimental arrangement. (b) X-ray image recorded *in situ* of an Al-20wt%Cu sample solidifying at a constant cooling rate of -0.025 K/s. FOV volume ≈ 2.9 × 2.9 × 0.2 mm. Low copper concentrations regions, e.g. solid equiaxed grains, appear lighter in the FOV, due to lower X-ray absorption. (c) Qualitative 3D reconstruction of the selected equiaxed grain shown in (b). *Z*-axis (*I*) shows gray level intensity.

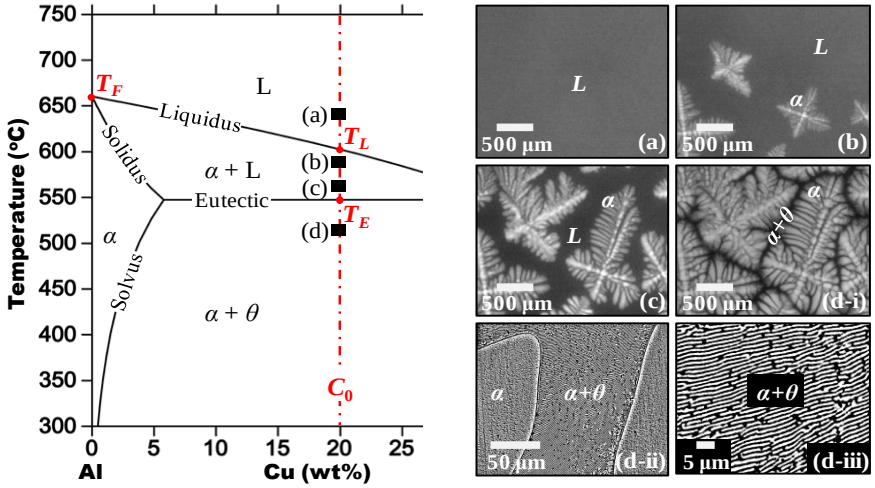

Figure 2. Hypoeutectic portion of the aluminium-copper phase diagram with Al-20wt%Cu alloy (C_0) selected. T_L and T_E denote the alloy liquidus and eutectic temperatures, respectively. Inset figures (a) to (d-i) show real-time *in situ* radiographs taken during a near-isothermal equiaxed solidification experiment, performed on a grain refined Al-20wt%Cu alloy, from the fully liquid to the fully solid state, respectively. Figures (d-ii) and (d-iii) show post mortem micrographs taken from a similar Al-20wt%Cu sample showing fine-scale eutectic microstructure. Sample solidified at cooling rates of -0.025 K/s and -1.0 K/s for equiaxed and eutectic growth, respectively. The micrographs recorded post-solidification at room temperature.

achieved due to the disparate X-ray absorption characteristics of the aluminium-rich crystals and the copper-rich liquid. Fig. 2(a) to (d-i) shows *in situ* X-ray images recorded relative to the temperatures indicated on the phase diagram, illustrating the (a) fully liquid (*L*), (b) semi-solid (α + *L*) at low solid fraction, (c) semi-solid at high solid fraction, and (d-i) the fully solid regimes (α + θ), respectively, demonstrating the random distribution of equiaxed grains, grain orientation, and morphology. Fig. 2(d-ii) and (d-iii) show optical micrographs of the solidified microstructure, showing the grain boundary eutectic structure at a magnification of approximately 10 times (d-ii) and 100 times (d-iii) the *in situ* image magnification. We have shown[7] that through combining *in situ* and post-mortem measurements, comparisons could be made to theoretical predictions of eutectic lamellar spacing.

In the following sections examples of two important features of solidification science recently analysed using *in situ* X-radiography are presented, thereby providing a demonstration of the applicability of real-time X-ray diagnostics in enhancing the materials science syllabus.

Solute Partitioning

A significant aspect of solidification, particularly with commonly used aluminium-based alloys, is solute partitioning, which can result in segregation within the as-cast macrostructure[11]. However, for *in situ* X-ray imaging, solute partitioning not only provides a means of clearly distinguishing between the solid and liquid phases, but also allows for measurement of solutal gradients in the liquid surrounding growing grains, which plays a significant role in crystal growth[12, 13]. Mathiesen *et al*.[14] showed results of interdendritic solutal rejection during directional solidification and the corresponding effect on dendrite tip growth velocity. Buffet *et al*.[15] presented quantitative solute profile measurements across a planar/dendritic interface during directional solidification experiments. Most recently, we have shown that, in cases where grain motion is severely limited, e.g. under microgravity conditions, physically separate equiaxed grains can become *solutally aware* of surrounding grains very early post-nucleation[9]. During solidification, as the primary phase α-Al forms in the Al-Cu liquid, copper solute is rejected from the α-Al solid into the liquid causing solute enrichment of the liquid surrounding the growing grain. If several growing grains exist within a liquid volume, as is normally the case, the solutal fields surrounding individual grains interact, resulting in a retardation of solid growth. This non-mechanical grain impingement is the mechanism by which grains can become *solutally aware*, as described previously.

Figure 3 shows the results of qualitative solute measurements taken from a near-isothermal equiaxed solidification experiment wherein equiaxed grain motion was suitably restricted so as to provide microgravity-like solidification conditions. Full details of the experimental apparatus and configuration have already been presented[8], and thus will only be described briefly herein. The X-ray diagnostics comprised a Viscom XT9100-T microfocus X-ray source and a Vosskuhler 11000 digital camera fitted with a Scint-*X* structured scintillator. The XRMON-GF gradient furnace, calibrated to near-isothermal mode, was used to melt/solidify the sample material. The thin sample (just 200 μm thick to enable X-ray penetration and contrast), seen in Figure 1, was Al-20wt%Cu alloy inoculated with 0.1wt%Al-Ti-B (5/1) grain refiner master alloy. Solidification was initiated through application of a constant cooling rate of 0.025 K/s for the initial primary solidification regime, i.e. equiaxed growth. Once primary growth had ceased (t > 545.5 s, Fig. 3), as observed in the X-ray FOV, the cooling rate was increased to 1.0 K/s for the remainder of solidification, including the eutectic trans-formation. The LH column of Fig. 3 shows the *in situ* images recorded during solidification; the RH column shows the corresponding solute profile measurements taken along the line profile $G_1 \rightarrow G_2$ – the length of the horizontal axis represents the distance between both points. The concentration profile was obtained by measuring the gray-level intensity, directly from the digital images, along the linear profile between points G_1 and G_2[12, 13]. The points G_1 and G_2 were arbitrarily selected as the grains-of-interest for this work, and represent the centre location of equiaxed nucleation for each grain. The dashed orthogonal lines originating from the G_1 and G_2 positions, respectively, represent the 2D primary arm growth axes. Note, all measurements were taken during post-processing of the image sequences.

At t = 0.0 s, prior to the onset of equiaxed nucleation, the fully liquid sample may be considered fully homogeneous, i.e. copper concentration of 20wt% throughout the FOV. To obtain a linear relationship between the gray-level intensity and the solute concentration, a region of fully eutectic solid was measured and assumed to contain 32.7wt%Cu[16]. A region of high α-Al solid, i.e. grain centre – see Fig. 1(c),

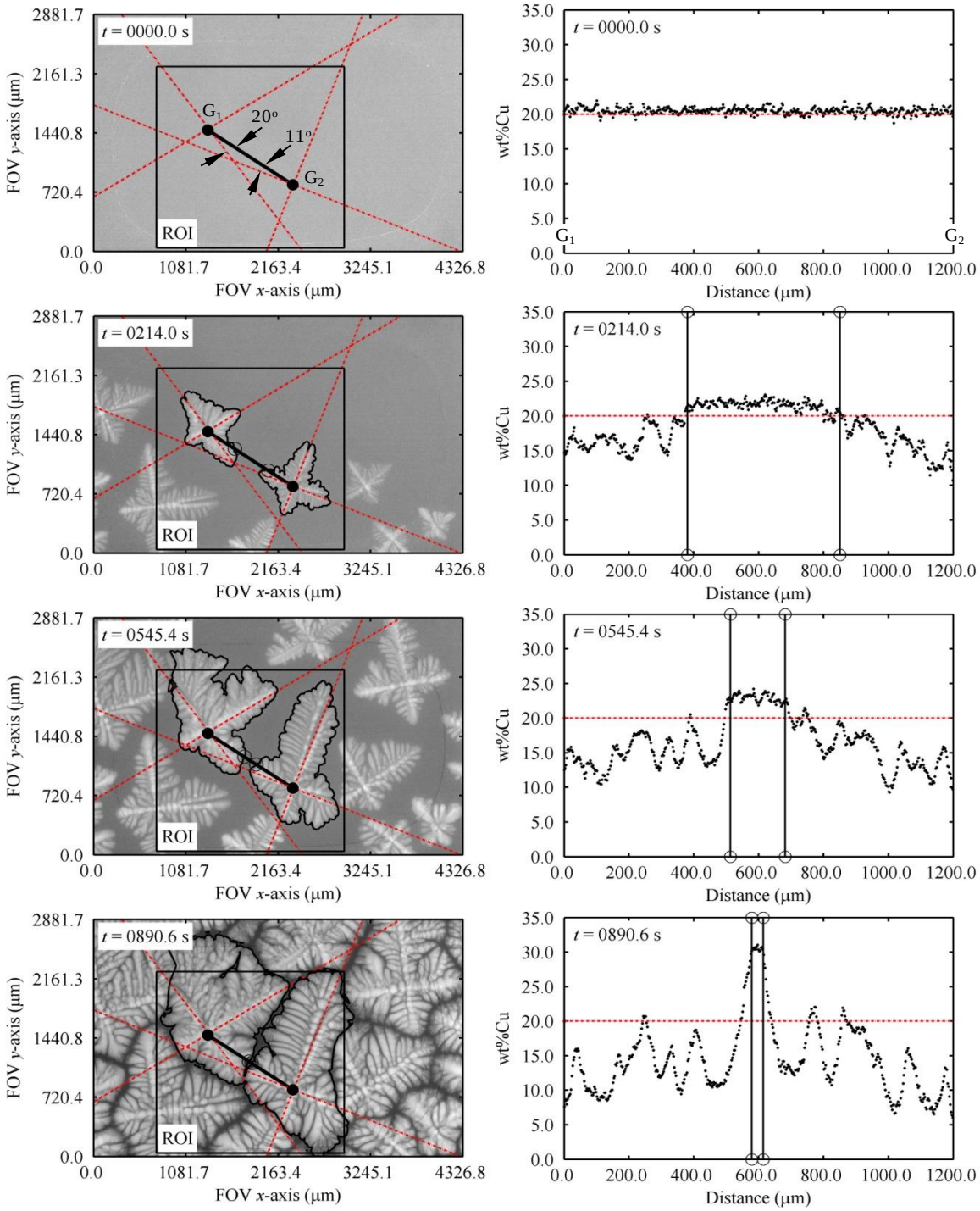

Figure 3. Al-20wt%Cu sample, inoculated with 0.1wt%Al-Ti-B (5/1) master alloy, near-isothermally solidified at a constant cooling rate of -0.025 K/s for the primary solidification phase and -1.0 K/s for the eutectic solidification phase. Points G_1 and G_2 show the nucleation centre location of two grains selected within the region or interest (ROI). The dashed lines indicate the grain orientations along their primary axes. The solid line connecting points G_1 and G_2 indicate the line of interest along which the qualitative copper concentration profile (wt%Cu) was measured. Solid boundary surrounding both grains represents the equiaxed grain envelope. Open circles show the intersection of the line of interest ($G_1 \rightarrow G_2$) and the grain envelopes.

was then measured and assumed to comprise an average concentration of ~6wt%Cu based on the solubility limit for α-Al and the ratio of α-Al to eutectic through the thickness of the sample at the location of the grain centre[8]. Note, assuming a linear relationship between gray-level intensity and solute concentration is not quantitatively correct in this case. In reality gray-level intensity is a function of the incident and transmitted X-ray energy, along with the absorption coefficient of the alloying elements[13,15,17]. Full details of the issues associated with quantitative concentration measurements using polychromatic laboratory-based *in situ* X-ray diagnostics have already been recorded[18] and, thus, will not be discussed further here. Critically, for the purposes of illustrating solutal interactions of separate grains, a linear approximation will be sufficient.

Examination of Fig. 3 shows that throughout solidification the intergranular liquid copper concentration continued to increase post-nucleation. However, due to the separation distance between grains, the solute concentration in the intergranular region appears to be relatively homogeneous, exhibiting a shallow concentration gradient. The copper concentration in the liquid further increased until the eutectic composition/temperature was reached resulting in the isothermal eutectic transformation at the end of solidification, giving rise to the visible grain boundaries. The relatively homogeneous copper enriched liquid resulted in a continuous decrease in the grain envelope growth velocities, as measured by Murphy *et al*.[9], until visible primary growth ceased and coarsening took over as the primary method of solid formation. Figure 3, although heretofore unpublished, is shown to our students. This early-view opportunity shows the benefits of research-informed education.

Gravity Effects

Figure 4 demonstrates the significant effect of gravity on equiaxed solidification, particularly in cases where high density differences exist between the solute (copper) and the solvent (aluminium). Both Fig. 4(a) and (b) were recorded using the same alloy (Al-20wt%Cu) and cooling rate (-0.025 K/s) and at the same temperature (~595 °C)[9]. Fig. 4(a) shows the evolving microstructure where equiaxed grain motion was severely limited, as discussed previously, thereby simulating microgravity-like solidification conditions[19]. Fig. 4(b) shows the more typical solidification conditions apparent during the industrial casting process, where gravity played a significant role during solidification and the resultant solidified grain structure. The technique used to achieve both solidification conditions is illustrated in Fig. 4(c), wherein the sample/X-ray source were positioned both parallel and perpendicular, respectively, to the action of gravity. In the former case, buoyant equiaxed grains were constrained to rest against the upper surface of the sample container (horizontal sample). In the latter case, buoyant grains were free to move in and out of the X-ray FOV as well as impinge upon one another (vertical sample).

Inspection of Figs. 4(a) and (b) shows a significant increase in the number of grains combined with a reduction in the average grain diameter, when comparing solidification in the presence of normal gravity effects (b) to solidification in the absence of significant gravity effects (a). Interestingly, there was little physical contact between individual grains in Fig. 4(a), throughout solidification, due to the relatively stationary solute fields surrounding each grain, leading to relatively large eutectic grain boundaries. However, significant grain motion during solidification shown in Fig. 4(b), resulted in grains physically impinging on surrounding grains, forming close-knit dendritic networks interspersed with large intergranular liquid voids. These results, when used as lecture content, helped us to demonstrate the physics underlying alloy solidification, which in turn control what happens in casting processes.

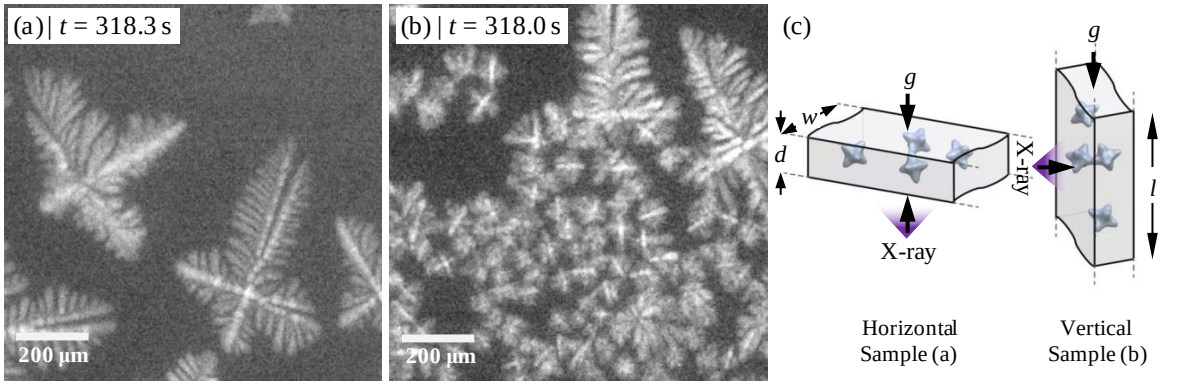

Figure 4. Al-20wt%Cu sample, inoculated with 0.1wt%Al-Ti-B (5/1) master alloy, near-isothermally solidified at a constant cooling rate of -0.025 K/s with the sample oriented horizontally (a) and vertically (b). Both (a) and (b) were recorded at approximately the same time/temperature after the onset of equiaxed nucleation. (c) Schematic illustration of the principle of sample orientation with respect to the action of gravity. In horizontally oriented samples equiaxed grain buoyancy is severely limited, exhibiting microgravity-like solidification conditions. Vertically oriented samples exhibit solidification conditions typical during foundry-based casting processes, i.e. normal casting conditions. Labels *w*, *d*, and *l* denote the sample width, depth, and length, in this case 5 × 0.2 × 50 mm, respectively.

CASTING PROCESSES

Students have learned the basic sand, investment, and permanent mold casting processes in earlier years in a Manufacturing Engineering course. Following study of alloy solidification, they are prepared for more advanced casting processes. Two case studies are presented in *Advanced Metals Processing*: one on semi-solid metal processing[20], the other on casting of functionally gradient materials[21]. In both cases the processes are those we have invented during experimental foundry research, and so we have a deep insight into their fundamentals of operation and key attributes. The semi-solid process studied is that of the Direct Thermal Method (DTM) of rheocasting, and the Cast Decant Cast (CDC) method is the process which can generate a gradient micro-structure in near net shape manufacture. In the first case, the primary advantage of DTM[22,23] is that it replaces a more complicated and expensive rheocasting process variant which requires active thermal management[24], without loss of capacity to generate unique (globular alloy primary phase) microstructures. CDC[25-28] on the other hand produces castings which cannot be made in any other way. The students are particularly engaged in engineering innovations which have been made within their University. The study of casting processes in which solidification of crystals occurs is then followed by learning about cooling of metal alloys to a solid in which no crystals are present: the bulk metallic glasses. Again, we have been carrying out research on this topic for a number of years now[29-31] and this enriches the learning experience for the students, who also carry out a laboratory practical on the subject.

PLASTICITY AND METAL FORMING

Metal forming is a major part of the curriculum, due to the relatively low cost of net shape processing and its ability to engineer microstructure into products. As is well known, the properties, deformation and microstructure of materials closely interact with one another as shown in Fig. 5.

While there have been extensive teaching activities covering the aforementioned three factors affecting metal forming, the computational prediction of materials microstructure, with metal deformation as input,

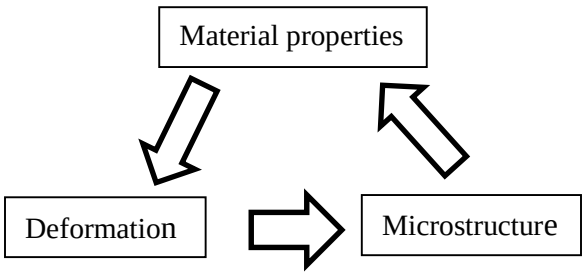

Figure 5. Interaction between the three major factors of metal forming.

is conventionally more a matter of research rather than a topic of teaching. However, in the current course, we highlight the computer modelling of microstructural evolution of materials in the process of metal rolling.

In a conventional hot rolling process for processing steel plates, phase transformation takes place in the solid state during cooling after the finish rolling stage. As the hot rolled steel plates cool down below Ae3 and above the eutectoid temperature, the chemical free energy of a low carbon steel favours a combination of austenite and ferrite in a two-phase microstructure resulting from the decomposition of the austenite matrix. By illustrating the schematic curves of the chemical free energy of the austenite-ferrite two-phase system as shown in Fig. 6, we help the students recall the related fundamentals of thermodynamics of alloys – including use of the regular solution model[32,33] to calculate the free energy of the phases based on their composition.

The driving force of the phase transformation is considered by taking into account the contributions of chemical free energy and grain/phase boundary energy. The Mesoscopic Monte Carlo model[34,35] has strong capability to predict the partition and diffusion of carbon and the corresponding transformation between austenite and ferrite phases. The Monte Carlo model mathematically discretizes the overall target material into an array of computational cells, as shown in Fig.7. Each cell carries related computational parameters, including such as phase status, composition, crystallographic orientation, dislocation density etc..

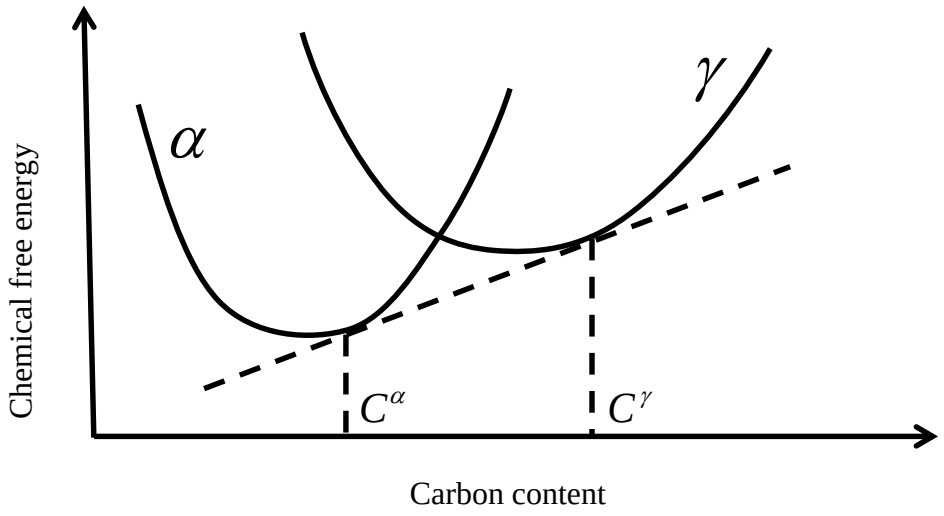

Figure 6. Schematic diagram showing the chemical free energy of the austenite-ferrite two-phase system of Fe-C binary alloy

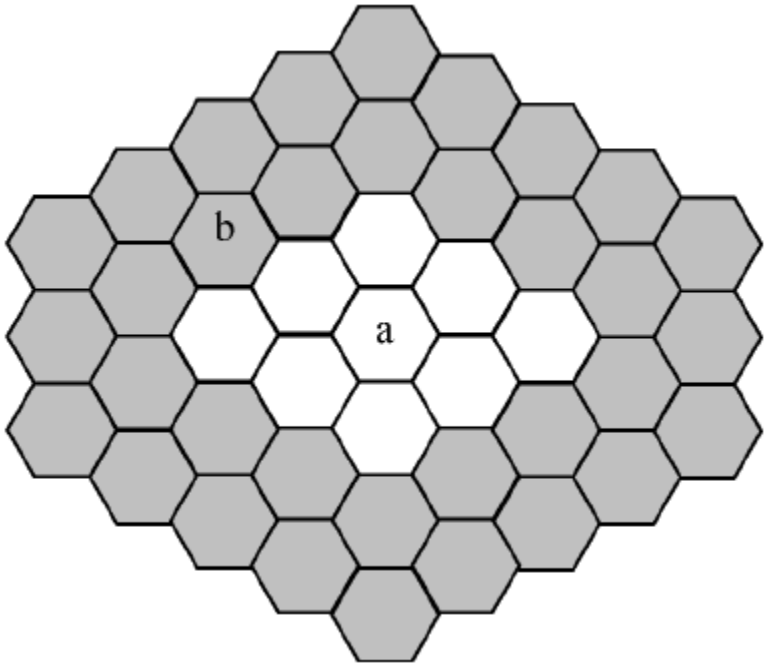

Fig.7 Schematic diagram of the computational cells that are used to discretize the target material, published in Ref. 36.

The core mechanism of this model inovolves statistically transiting the state of computational cells of the target material at every time step of computation, depending on the physical processes dominating. The transition of state (e.g. either austenite phase or ferrite phase) of a computational cell is determined by the probability of transition, *W*, of:

$$W = \begin{cases} 1, \Delta G \le 0 \\ \exp(-\dfrac{\Delta G}{kT}), \Delta H > 0 \end{cases} \quad (1)$$

where ΔG is the increase of Gibbs free energy of the system, *k* is Boltzmann's constant and *T* is temperature. This means that the transition of state (e.g. from austenite to ferrite) is definitely successful if it results in the decrease of Gibbs free energy of the material, in the computation. Otherwise, there is only a relatively low probability of success, depending on the absolute value of ΔG and the temperature. The value of ΔG can be affected by a variety of dominant microscopic processes, including solute partition/diffusion and crystal lattice transformation, such that:

$$G = E_C + E_B \quad (2)$$

where E_C is the chemical free energy depending on the composition and phase of the grains, and E_B can be the grain boundary energy - depending on the grain misorientation. By using appropriate mathematics for the chemical free energy (e.g. regular solution model) and grain/phase boundary energy[34,35], the mesoscopic Monte Carlo model predicts reasonably well the morphology, composition, and fraction of the ferrite and austenite phases at equilibrium (shown in Fig.8). Besides a good agreement in the morphology of grains between the simulation result and experimental measurement as shown in Fig. 8, we demonstrate

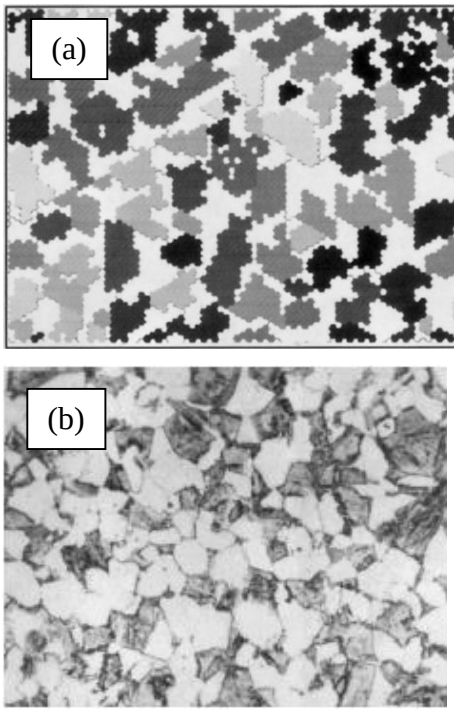

Figure 8. Morphology of the austenite (dark) - ferrite (light) two-phase system predicted by the Monte Carlo simulation (a) and characterized by the optical metallography in experiment (b), as published in Ref. 34..

that the calculated volume fraction and composition of the ferrite and austenite phases by the Monte Carlo model at equilibrium quantitatively agree well with the Fe-C binary phase diagram[34].

By learning the basics of computational methods for the austenite-to-ferrite phase transformation, the students become familiar with simulation of the solid state phase transformation in the continuous cooling process of hot rolled steel plates or in the annealing of cold rolled steel strips.

Based on this stepping stone example of Monte Carlo modelling, we illustrate to students that the driving force for the phase transformation can be modified by including the contribution of deformation energy that is stored in the deformed material in the form of dislocations. Such stored energy can drive the transformation from the austenite phase to the ferrite phase at a temperature that is even higher than Ae3, in the process of finish rolling. This type of transformation is called deformation induced ferrite transformation (DIFT)[37], which has strong potential to dramatically refine the microstructure of hot rolled materials.

By considering the contribution of the stored energy of deformation (E_D) in the free energy of the system via:

$$G = E_C + E_B + E_D , \qquad (3)$$

the Monte Carlo model[36,38] for the DIFT was developed. In the class, the students can clearly see its use in predicting the microstructural change of the carbon steel due to DIFT during hot rolling, by reviewing our paper via Fig. 9. Significant plastic deformation of the material due to hot rolling can lead to a comparatively large value of E_D . At a certain temperature, the phase transformation from the highly deformed austenite matrix to the almost dislocation free ferrite can lead to a relatively negative value of ΔG , and hence DIFT proceeds (according to Eq.1) in simulations shown in Fig.8. In the class, the students not only acquire a mesoscopic computational method for predicting the microstructure of alloys, but also and more importantly learn the important influence of macroscopic deformation on the resultant microstructure of materials.

Besides the Monte Carlo model, we also introduce cellular automata models for predicting the normal grain growth[39] and recrystallization[40] of materials. These are the competitors of the Monte Carlo model in the field of modelling materials microstructure. In total, the students learn about computational methods for predicting materials microstructure in hot metal rolling, including the grain growth between the reheating in a furnace and primary rolling, the recrystallization in the process of primary and finish rolling, and the solid state phase transformation in the process of finish rolling and continuous cooling as shown in Fig. 10. Learning about these models not only makes the students familiar with a selection of powerful

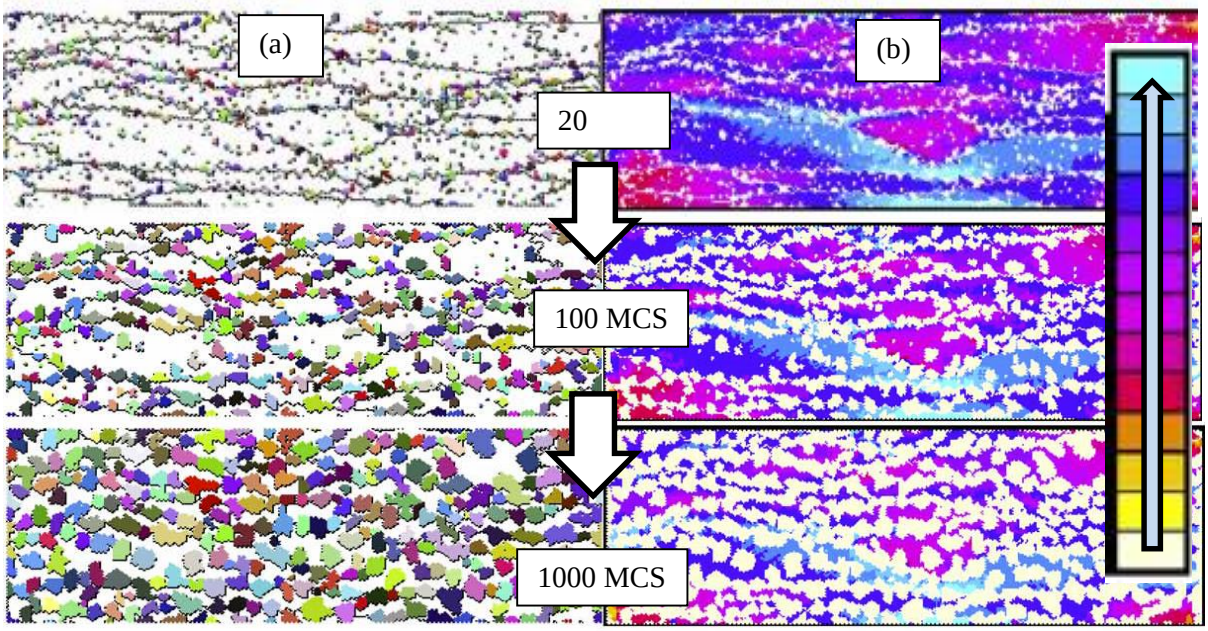

Figure 9. Consecutive evolution of (a) the microstructure and (b) the stored energy of deformation, in a deformed (strain 0.9) sample of low carbon steel[38]. In the microstructure of column (a), the color (shade in black and white reproduction) represents the orientation of ferrite grains and the white matrix represents the austenite grains. In Column (b), the color scale represents the level of stored energy of deformation. The time is in the unit of Monte Carlo steps (MCS). The rolling has reduced the thickness of the material from the top and bottom boundaries of the simulation domain, and hence the grains of austenite matrix are elongated along the horizontal direction. There are no changes to the thickness of the workpiece from (a) through (c); rather only micostructural eveolution with time in the as-rolled alloy.

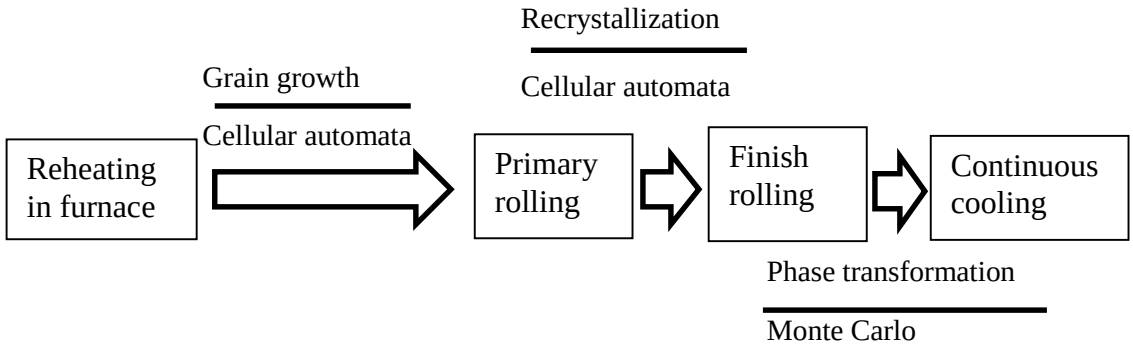

Figure 10. Phenomena and corresponing computational models applied at different stages of continuous hot metal rolling process

computational tools, but also helps them develop an insight into the underlying physics of related phenomena. For example, in order to properly formulate the mathematics of the driving force for the phase transformation of the target system (e.g. Eq.3), the students have to understand the governing physics of phenomena such as evolution of dislocations, diffusion of solute, presentation of grain/phase boundaries, and crystal lattice transformation.

In their potential careers in materials processing, the students will recall the importance of optimising the materials microstructure when

they design the operational parameters of specific metal forming processes. If they become materials scientists or engineers in the future, they can use such computational models to study the metallurgy of the formed materials. Compared with conventional teaching courses on metal forming, we highlight to our students the influence of the deformation on resultant microstructure. In this way we ensure that the students will bear in mind that metal forming is not only a matter of deformation of materials but also entails a dramatic change of the materials microstructure. This learning outcome has been achieved by reference to the research experience of one of the authors. The insight gained in considering the formulation of the computational model, and its execution, helps the students develop understanding of key process metallurgy principles.

OUTCOMES AND DISCUSSION

The student response to the course has been largely positive. This is elicited via a University-wide on-line system of surveying students for all taught modules. The standard 5 statements posed are:

a. I have a better understanding of the subject after completing this module.
b. The assessments to date were relevant to the work of the module.
c. I achieved the learning outcomes for this module.
d. The teaching on this module supported my learning.
e. Overall I am satisfied with this module.

Responses are sought using the Likert Scale, with scoring (number in brackets) from 1 through 5 for each of the following responses, respectively: Strongly Disagree (1); Disagree (2); Not Sure (3); Agree (4); Strongly Agree (5). Thus, responses with average scores above 4 are very positive. In 2015, when the *Advanced Metals Processing* module was last taught in the manner described in this paper, the average scores were: a: 4.67, b: 4.33, c: 4.00; d: 4.67, e: 4.33. In comparison, the average scores for all taught modules across the School of Mechanical and Materials Engineering were: 4.18, 4.13, 3.99, 3.92 and 3.94 for a. to e., respectively. This shows that the students have a high opinion of our research-led course, with comments such as "interesting material from clear experts" and "material appears up to date" included in response to open-ended questions in the survey. The numbers taking the module has also increased, from 12 in 2014, to 16 in 2015, to (currently) 30 in 2016. However this reflects an increase in overall enrolment in a new Masters degree programme in Materials Science and Engineering at UCD, so is not wholly down to increased popularity of the module. Having said that, the module is also being taken by students majoring in Mechanical Engineering, and Biomedical Engineering.

CONCLUSIONS

We have shown that teaching and learning can be enhanced by a portfolio of active related research, and that members of a typical research group can form an effective team for teaching an up-to-date curriculum to a larger group of senior university students. The incorporation of research findings, both published and unpublished, makes the course content contemporary, and with a local flavor. In this way, students are equipped with knowledge of state-of-the art in the subject, which in this case is the near net shape processing of metallic alloys. The outcomes are positive, as attested to by the students' feedback via on-line surveys.

REFERENCES

1. V. Gordon Childe, The Bronze Age, Oxford University Press on behalf of the Past and Present Society, no. 12, pp. 2–15, 1957.
2. R. Mallet, On the Physical Conditions Involved in the Construction of Artillery, . Longmans, Brown, Green, Longmans, and Roberts, London, 1856.
3. B. Chalmers, Principles of Solidification. Wiley, New York, 1964.

4. R. Mathiesen, L. Arnberg, H. Nguyen-Thi, and B. Billia, JOM, **64**, 76 (2012).
5. H. Nguyen-Thi, L. Salvo, R. H. Mathiesen, L. Arnberg, B. Billia, M. Suery, and G. Reinhart, *Comptes Rendus Physique*, **13**, 237 (2012).
6. H. Nguyen-Thi, G. Reinhart, G. Salloum Abou Jaoude, R. H. Mathiesen, G. Zimmermann, Y. Houltz, D. Voss, A. Verga, D. J. Browne, and A. G. Murphy, *J. Cryst. Growth*, **23–30** 374 (2013).
7. J.-O. Andersson, T. Helander, L. Höglund, P. Shi, and B. Sundman, *Calphad*, **26**, 273 (2002).
8. A. G. Murphy, D. J. Browne, W. U. Mirihanage, and R. H. Mathiesen, *Acta Mater.*, **61**, 4559 (2013).
9. A. G. Murphy, W. U. Mirihanage, D. J. Browne, and R. H. Mathiesen, *Acta Mater.*, **95**, 83 (2015).
10. H. Nguyen-Thi, G. Reinhart, G. Salloum-Abou-Jaoude, D. J. Browne, A. G. Murphy, Y. Houltz, J. Li, D. Voss, A. Verga, R. H. Mathiesen, and G. Zimmermann, *Microgravity Sci. Tech.*, **26**, (2014).
11. W. Kurz and D. J. Fisher, *Fundamentals of Solidification, 3rd ed.*, Trans Tech Publications, Aedermannsdorf, Switzerland: 1989.
12. S. McFadden, P. L. Schaffer, R. H. Mathiesen, and D. J. Browne, *Mater. Sci. Forum*, **654–656**, 1359 (2010).
13. A. Bogno, H. Nguyen-Thi, G. Reinhart, B. Billia, and J. Baruchel, *Acta Mater.*, **61**, 1303 (2013).
14. R. H. Mathiesen, L. Arnberg, K. Ramsøskar, T. Weitkamp, C. Rau, and A. Snigirev, *Metall. Mater. Trans. B*, **33**, 613 (2002).
15. A. Buffet, H. Nguyen-Thi, A. Bogno, T. Schenk, N. Mangelinck-Noël, G. Reinhart, N. Bergeon, B. Billia, and J. Baruchel, *Mater. Sci. Forum*, **649**, 331 (2010).
16. H. Baker and H. Okamoto, Eds., *ASM Handbook*, Vol. 03 - Alloy Phase Diagrams. ASM International, 1992.
17. W. U. Mirihanage, K. V. Falch, I. Snigireva, A. Snigirev, Y. J. Li, L. Arnberg, and R. H. Mathiesen, *Acta Mater.*, **81**, 241 (2014).
18. A. G. Murphy, "In Situ X-Ray Monitoring of Advanced Alloy Solidification Processes under Microgravity and Terrestrial Conditions," PhD Thesis, University College Dublin (Ireland), 2013.
19. A. G. Murphy, J. Li, O. Janson, A. Verga, and D. J. Browne, *Mater. Sci. Forum*, **790–791**, 52–58 (2014).
20. H.V. Atkinson, *Materials Science & Technology*, **26**, 1401 (2010)
21. B. Anandavel, S.S. Mohamed Nazirudeen, J. Anburaj and P.C. Angelo, *Transactions of the Indian Institute of Metals*, **68 (Suppl. 2)**, S137 (2015).
22. D.J. Browne, M.J. Hussey, A.J. Carr and D. Brabazon, *International Journal of Cast Metals Research*, **16**, 418 (2003).
23. A.J. Carr, D.J. Browne, M.J. Hussey, N. Lumsden and M. Scanlan, *International Journal of Cast Metals Research*, **20**, 325 (2007).
24. M.A. Easton, H. Kaufmann, W. Fragner, *Mater. Sci. Eng. A*, **420**, 135 (2006).
25. M. Scanlan, D.J. Browne, and A. Bates, *Mater. Sci. Eng. A*, **413-414**, 66 (2005).
26. D. Browne, S. Kelly, P. Tiernan, A. Bates, M. Scanlan, "A Method for Producing a Functionally Gradient Component", US Patent 7,874,344 (2011)
27. S.P. Midson and D.J. Browne, *Advanced Materials and Processes*, **166** (10), 38, (2008).
28. S.P. Midson and D.J. Browne, *Solid State Phenomena* ,**191-193**, 506 (2012).
29. D.J. Browne, Z. Kovacs and W.U. Mirihanage, *Transactions of the Indian Institute of Metals*, **62** (4-5), 409 (2009).
30. D.J. Browne, D. Stratton, M.D. Gilchrist, and C. Byrne, *Metallurgical & Materials Transactions A*, **44**, 2021 (2013).
31. A.P. Srivastava, T. Stefanov, D. Srivastava,

and D.J. Browne, *Mater. Sci. Eng. A*, **651**, 69 (2016).

32. J. H. Hildebrand and R. L. Scott, Regular Solutions, Prentice-Hall, Englewood Cliffs, N.J., 1962.
33. J. H. Hildebrand, J. M. Prausnitz, and R. L. Scott, "*Regular and Related Solutions*", Van Nostrand Reinhold Co., New York, 1970
34. M. Tong, D.Z. Li, Y.Y. Li and J. Ni, *Metall. Mater. Trans. A*, **33**, 3111 (2002).
35. M. Tong, D.Z. Li and Y.Y. Li, *Acta Mater.*, **53**, 1485 (2005).
36. M. Tong, J. Ni, Y. Zhang, D.Z. Li and Y.Y. Li, *Metall. Mater. Trans. A*, **35**, 1565 (2004).
37. Y.Q. Weng, *ISIJ International*, **43**, 1675 (2003).
38. N. Xiao, M. Tong, Y. Lan, D.Z. Li and Y.Y. Li, *Acta Materialia*, **54**, 1265 (2006).
39. S. Raghavan, and Satyam S. Sahay, *Mater. Sci. Eng. A*, **445–446**, 203 (2007).
40. H. W. Lee and I. Yong-Taek, *International Journal of Mechanical Sciences*, **52**, 1277 (2010).